

Atomic Layer Deposition of Tungsten Nitride Films Using Sequential Surface Reactions

J. W. Klaus, S. J. Ferro, and S. M. George^z

Department of Chemistry and Biochemistry, University of Colorado, Boulder, Colorado 80309, USA

Tungsten nitride films were deposited with atomic layer control using sequential surface reactions. The tungsten nitride film growth was accomplished by separating the binary reaction $2\text{WF}_6 + \text{NH}_3 \rightarrow \text{W}_2\text{N} + 3\text{HF} + 9/2\text{F}_2$ into two half-reactions. Successive application of the WF_6 and NH_3 half-reactions in an ABAB... sequence produced tungsten nitride deposition at substrate temperatures between 600 and 800 K. Transmission Fourier transform infrared (FTIR) spectroscopy monitored the coverage of WF_x^* and NH_y^* surface species on high surface area particles during the WF_6 and NH_3 half-reactions. The FTIR spectroscopic results demonstrated that the WF_6 and NH_3 half-reactions were complete and self-limiting at temperatures ≥ 600 K. *In situ* spectroscopic ellipsometry monitored the film growth on Si(100) substrates vs. temperature and reactant exposure. A tungsten nitride deposition rate of 2.55 Å/AB cycle was measured at 600-800 K for WF_6 and NH_3 reactant exposures ≥ 3000 L and 10,000 L, respectively. X-ray photoelectron spectroscopy depth-profiling experiments determined that the films had a W_2N stoichiometry with low C and O impurity concentrations. X-ray diffraction investigations revealed that the tungsten nitride films were microcrystalline. Atomic force microscopy measurements of the deposited films observed remarkably flat surfaces indicating smooth film growth. These smooth tungsten nitride films deposited with atomic layer control should be useful as diffusion barriers for Cu on contact and via holes.

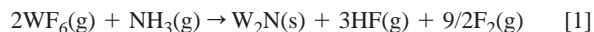
© 2000 The Electrochemical Society. S0013-4651(99)05-028-4. All rights reserved.

Manuscript submitted May 6, 1999; revised manuscript received November 21, 1999.

The deposition of diffusion barriers is an important processing challenge in semiconductor device manufacturing.¹ Diffusion barriers become increasingly important as device dimensions approach the nanometer scale and the need to prevent intralayer and dopant diffusion becomes more urgent. Refractory metal nitrides are leading candidates for diffusion barriers because of their high stability at temperatures $>450^\circ\text{C}$.² In particular, tungsten nitride has generated considerable interest because tungsten nitride is an excellent barrier for Cu diffusion into Si at elevated temperatures.^{3,4} The conformal deposition of ultrathin tungsten nitride films on high aspect ratio structures is required for the most critical applications. Ultrathin tungsten nitride deposition on contact holes is necessary to prepare stable Cu/Si contacts with extremely low resistance.^{2,5,6} Conformal tungsten nitride deposition on via holes of multiple level interconnects is needed to provide a barrier for Cu diffusion into SiO_2 or other low k dielectrics.^{5,6}

Self-terminating surface reactions applied in a sequential manner can be used to achieve conformal and atomic layer controlled thin film growth.⁷⁻⁹ This sequential surface reaction approach has been used to grow a variety of oxide,¹⁰⁻¹⁴ nitride,¹⁵ sulfide,¹⁶ and phosphide¹⁷ thin films. Smooth single-element metallic tungsten thin films have also been deposited recently with atomic layer control.¹⁸ Atomic layer controlled growth using sequential surface reactions is ideal for precise and conformal deposition on both flat and high aspect ratio structures. This method is known to produce pinhole-free films and is easily extended to large substrate areas.

The thermal chemical vapor deposition (CVD) reaction



has been used previously to deposit tungsten nitride.^{19,20} Plasma-enhanced CVD with WF_6 and NH_3 has also been employed to grow tungsten nitride films.^{6,21-23} To deposit tungsten nitride films with atomic layer control, the thermal CVD reaction was split into the following two half-reactions



The asterisks in the above reactions designate the surface species. The stoichiometry is kept indefinite because our surface chemistry studies indicate that there are several possible reaction pathways.

In each half-reaction, the WF_x^* and WNH_y^* surface species react with the gas-phase precursors. The surface reactions continue until all of the initial surface species have been converted to new surface species and volatile product molecules. The surface reactions self-terminate after the consumption of all the initial surface species and additional reactant exposure results in no additional growth. Application of the half-reactions in a ABAB... reaction sequence results in atomic layer deposition. If the surface half-reactions are allowed to reach completion everywhere on the substrate, changes in reactant pressure or total reactant exposure will not change the growth per AB cycle.⁷

The atomic layer deposition of tungsten nitride was investigated using two sets of experiments. In the first set of experiments, *in situ* transmission Fourier transform infrared (FTIR) spectroscopy experiments were performed on high surface area particles to monitor the surface chemical reactions during the tungsten nitride film growth. The coverages of WF_x^* and NH_y^* surface species were monitored vs. time by observing the W-F_x stretching mode and the N-H_y stretching and bending modes. In the second set of experiments, tungsten nitride films were deposited on Si(100) substrates and examined using *in situ* spectroscopic ellipsometry. The ellipsometry measurements determined the tungsten nitride film thickness and index of refraction vs. deposition temperature and reactant exposure.

These two sets of experiments revealed that atomic layer controlled growth of tungsten nitride can be attained using sequential exposures to WF_6 and NH_3 . Additional atomic force microscopy studies characterized the flatness of the tungsten nitride films relative to the initial Si(100) substrate. The tungsten nitride film properties were also evaluated by X-ray photoelectron spectroscopy (XPS) depth-profiling to determine film stoichiometry and X-ray diffraction experiments to ascertain film structure. These studies all indicate that atomic layer deposition techniques should be useful in depositing ultrathin and conformal tungsten nitride diffusion barriers in semiconductor device fabrication.

Experimental

FTIR spectroscopy studies on silica powder.—The FTIR spectroscopy experiments were conducted in a high vacuum chamber designed for *in situ* transmission FTIR spectroscopic investigations.²⁴ A schematic of this apparatus is shown in Fig. 1. The chamber has a base pressure of 5×10^{-8} Torr. The chamber is equipped with a 200 L/s turbomolecular pump, CsI windows, a Bayard-Alpert ionization gauge, a capacitance manometer, and a Dycor quadrupole mass spectrometer. The vibrational spectra were recorded with a

^z E-mail: Georges@Spot.Colorado.Edu

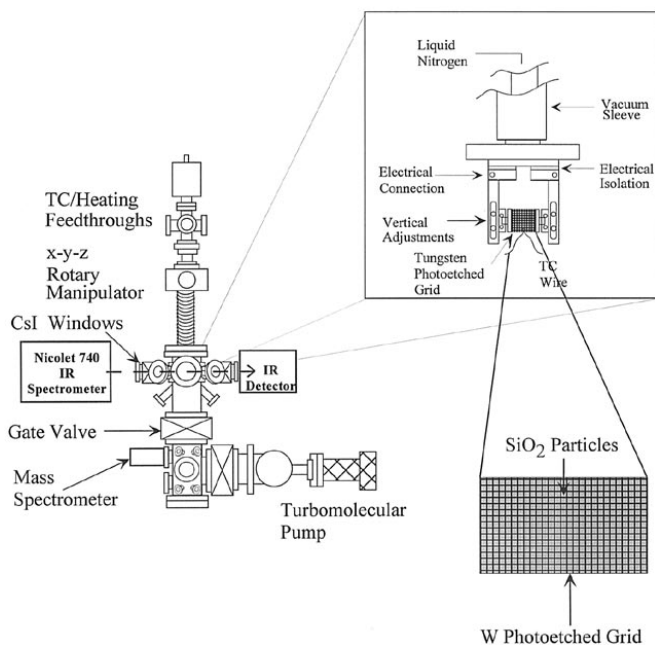


Figure 1. Experimental schematic of vacuum chamber for transmission FTIR studies on high surface area samples. SiO₂ particles with a surface area of 380 m²/g are pressed into a tungsten grid and positioned in the infrared beam.

Nicolet 740 FTIR spectrometer and an MCT-B detector. To achieve sufficient surface sensitivity, high surface area silica powder (Aldrich fumed silica, 380 m²/g) was pressed into a tungsten photoetched screen (Buckbee-Mears, 100 LPI, 0.002 in. thick) and suspended between copper posts on the sample mount.²⁵ This sample could be resistively heated to ~1000 K.

The IR spectrum of the silica powder recorded immediately after loading into vacuum exhibited a pronounced surface vibrational feature that extended from 3750–3000 cm⁻¹. This feature is attributed to SiOH* surface species.²⁶ The hydroxylated SiO₂ surface is very stable and does not react directly with WF₆.²⁷ To facilitate the nucleation of the tungsten nitride films, the SiO₂ surface was first exposed to 10 Torr of SiCl₄ at 600 K for 30 min. This reaction produced a Cl-terminated SiO₂ surface characterized by a strong Si-Cl stretching vibration at ~650 cm⁻¹.²⁶

The surface terminated with SiCl* species was further exposed to 10 Torr of NH₃ at 700 K for 30 min. This reaction results in replacement of the SiCl* species with SiNH₂* amino groups.¹⁵ The SiNH₂* amino groups were then allowed to react with ~1 Torr of WF₆ for 30 min. This reaction produced a surface terminated with WF_x* species. A few WF₆ and NH₃ reaction cycles were subsequently performed on this surface to transform the SiO₂ surface into a tungsten nitride surface. The WF₆ and NH₃ surface reactions were examined on this tungsten nitride surface.

Transmission FTIR spectroscopy was utilized to measure the WF_x* species and NH_y* species during the WF₆ and NH₃ half-reactions. The FTIR spectra were recorded at 340 K after various WF₆ or NH₃ exposures at different temperatures. Gate valves protected the CsI windows during the reactant exposures. The WF_x* surface species were monitored using the W-F stretching mode located at ~680 cm⁻¹.²⁸ The NH_y* surface species were monitored by observing the dominant N-H₂ stretching modes and N-H₂ scissors mode centered at ~3400 and 1500 cm⁻¹, respectively.²⁹⁻³¹

Spectroscopic ellipsometry studies on Si(100).—The tungsten nitride film growth experiments were performed in a high vacuum apparatus that has been described in detail elsewhere.¹⁰ A schematic of this experimental setup including the *in situ* ellipsometer is illustrated in Fig. 2. In brief, the apparatus consists of a sample load lock chamber, a central deposition chamber, and an ultrahigh vacuum chamber for surface analysis. The central deposition chamber is

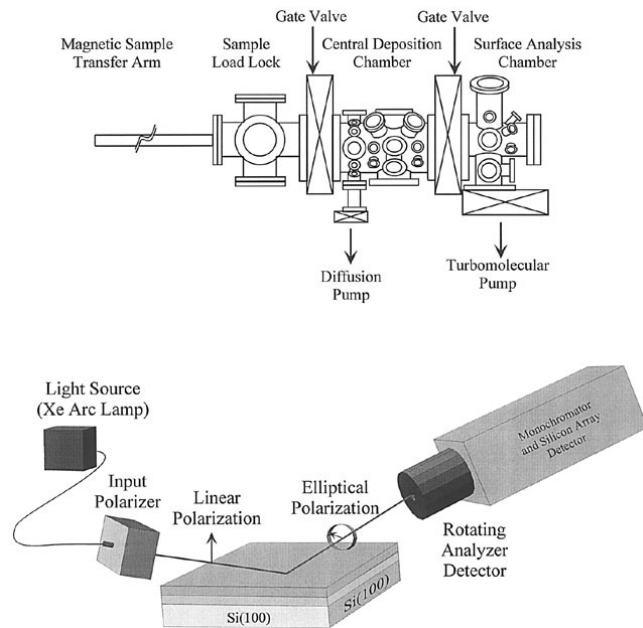


Figure 2. Experimental schematic of vacuum apparatus for *in situ* spectroscopic ellipsometry studies on Si(100) samples. This apparatus contains a sample load lock, a central deposition chamber equipped with the spectroscopic ellipsometer, and a surface analysis chamber.

capable of automated dosing of molecular precursors under a wide variety of conditions. The deposition chamber is pumped with either a 175 L/s diffusion pump backed by a liquid N₂ trap and a mechanical pump or two separate liquid N₂ traps backed by mechanical pumps. This chamber has a base pressure of 1 × 10⁻⁷ Torr.

The central deposition chamber is equipped with an *in situ* spectroscopic ellipsometer (J.A. Woolam Co. M-44) that collects ellipsometric data at 44 visible wavelengths simultaneously. The spectroscopic ellipsometric measurements determined the refractive index and thickness of the tungsten nitride films using a Lorentz oscillator model.^{32,33} The 88 data points (Ψ and Δ for the 44 individual wavelengths) were fit using two oscillators and the film thickness. Each oscillator has a central energy, amplitude, and width. The weak coupling between the real and imaginary refractive index ($\tilde{n} = n + ik$) and the thickness allowed the unique determination of these parameters.

The ellipsometer is mounted on the central deposition chamber employing ports positioned at 80° with respect to the surface normal. Gate valves protect the birefringent-free ellipsometer windows from deposition during the WF₆ and NH₃ exposures. The surface analysis chamber contains a UTI-100C quadrupole mass spectrometer and a Bayard-Alpert ionization gauge. Mass spectrometric analysis of the gases in the central deposition chamber is performed using a controlled leak to the surface analysis chamber. The surface analysis chamber is pumped by a 210 L/s turbomolecular pump to obtain a base pressure of 1 × 10⁻⁹ Torr.

The sample substrate was a Si(100) wafer covered with 125 Å of SiO₂ formed by thermal oxidation. The Si(100) wafers were p-type boron-doped with a resistivity of $\rho = 0.01\text{--}0.03 \Omega \text{ cm}$. Square pieces of the Si(100) wafer with dimensions of 0.75 × 0.75 in. were used as the samples. The highly doped Si(100) samples were suspended between copper posts using 0.25 mm Mo foil and could be resistively heated to >1100 K. The sample temperature was determined by a Chromel-Alumel thermocouple pressed onto the SiO₂ surface using a spring clip.

The Si(100) samples were cleaned with methanol, acetone, and distilled water before mounting and loading into the chamber. The SiO₂ surface was further cleaned in vacuum by an anneal at 900 K for 5 min. This thermal anneal was followed by a high frequency H₂O plasma discharge at 300 K. This H₂O plasma fully hydroxylated the SiO₂ surface and removed surface carbon contamination.

To initiate the tungsten nitride film growth, the hydroxylated SiO₂ surface was first exposed to 10 mTorr of Si₂H₆ at 600 K for ~5 min. Under these conditions, FTIR spectroscopy indicates that Si₂H₆ reacts with the surface hydroxyl groups and deposits surface species containing Si-H stretching vibrations: e.g., SiOH* + Si₂H₆ → SiOSiH₃* + SiH₄. After the initial Si₂H₆ treatment, tungsten nitride film growth could be performed at reaction temperatures between 550-800 K. A few WF₆ and NH₃ reaction cycles were utilized to transform the SiO₂ surface to a tungsten nitride surface. The dependence of the tungsten nitride growth rate on WF₆ and NH₃ reactant exposure was examined on this tungsten nitride surface.

Results

FTIR spectroscopy studies of surface chemistry.—Several infrared difference spectra recorded during the NH₃ half-reaction at 600 K are displayed in Fig. 3. These infrared difference spectra are referenced to a tungsten nitride surface that had earlier received a saturation exposure of WF₆ at 600 K. The spectra after various NH₃ exposures are offset for clarity in presentation. The infrared spectra show N-H₂ stretching vibrations at ~3450 cm⁻¹ and N-H₂ scissors vibrations at ~1500 cm⁻¹. These results indicate that the NH₂* surface species is primarily a NH₂* surface species. The infrared spectra also display W-F_x stretching vibrations at 680 cm⁻¹. The spectra reveal a gradual increase in the dominant NH₂* surface species that is coupled with a corresponding loss in WF_x* surface species vs. NH₃ exposure. The loss of WF_x* surface species appears as a negative absorbance.

Figure 4 displays infrared difference spectra recorded during the subsequent WF₆ exposure at 600 K. The difference spectra are again offset to display the changes vs. WF₆ exposure. Each difference spectrum displays the change in the infrared absorbance referenced to a tungsten nitride surface that had received a saturation NH₃ exposure at 600 K. The gain of WF_x* surface species is concurrent with a loss of NH₂* surface species. The loss of NH₂* surface species appears as a negative absorbance.

The normalized integrated absorbances during the NH₃ and WF₆ half-reactions are displayed in Fig. 5. The loss of WF_x* surface species during the NH₃ half-reaction occurs more rapidly than the corresponding gain of the NH₂* surface species. This behavior indi-

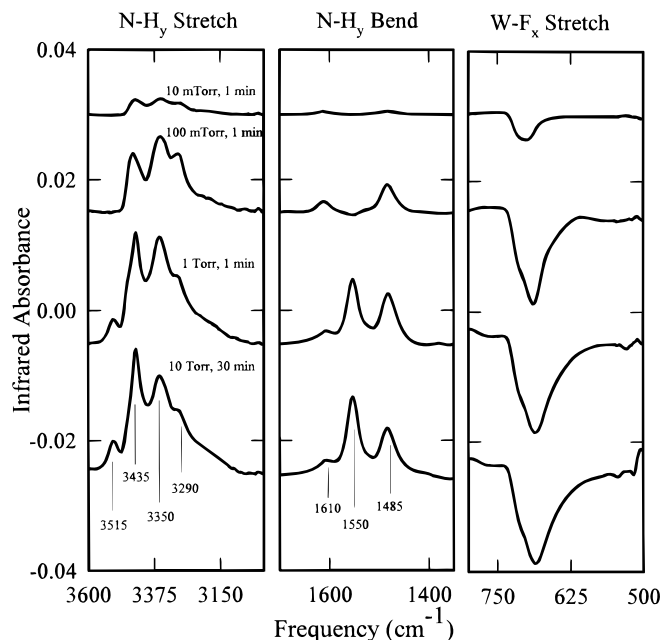


Figure 3. FTIR difference spectra in the N-H₂ stretch, N-H₂ bend, and W-F_x stretch regions recorded after various NH₃ exposures during the NH₃ half-reaction at 600 K. Each difference spectrum is referenced to a surface that had earlier received a saturation WF₆ exposure at 600 K.

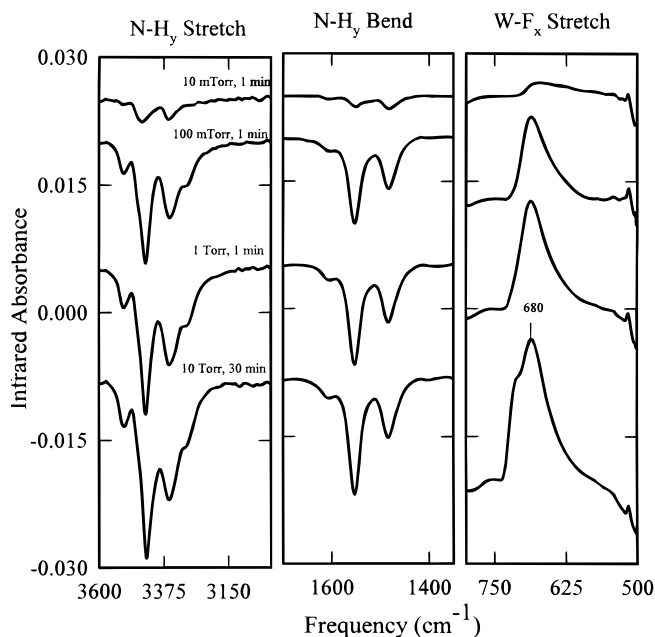


Figure 4. FTIR difference spectra in the N-H₂ stretch, N-H₂ bend, and W-F_x stretch regions recorded after various WF₆ exposures during the WF₆ half-reaction at 600 K. Each difference spectrum is referenced to a tungsten nitride surface that had earlier received a saturation NH₃ exposure at 600 K.

cates that each NH₃ molecule may initially react with multiple WF_x* surface species. In contrast, the gain of WF_x* surface species during the WF₆ half-reaction is concurrent with the loss of NH₂* surface

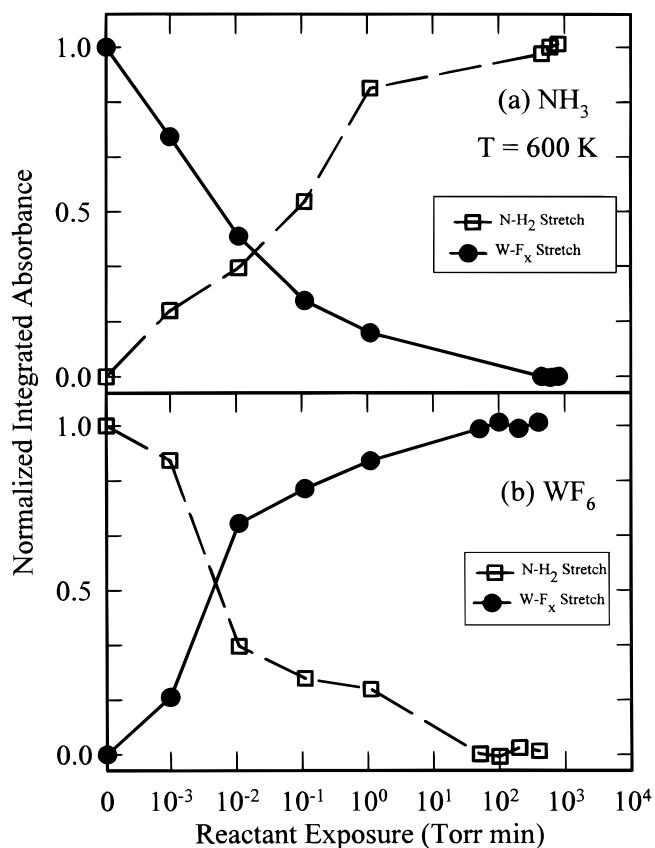


Figure 5. Normalized integrated absorbances for the W-F_x stretching mode (~680 cm⁻¹) and the N-H₂ stretching mode (~3400 cm⁻¹) vs. reactant exposure during the (a) NH₃ and (b) WF₆ half-reactions at 600 K.

species. This behavior indicates a 1:1 reaction between WF_6 and NH_2^* surface species.

The loss of NH_2^* surface coverage during the WF_6 half-reaction results in the growth of WF_x^* surface coverage. When the WF_6 half-reaction reaches completion, this WF_x^* surface coverage is equivalent to the WF_x^* surface coverage measured prior to the NH_3 half-reaction. Similarly, the loss of WF_x^* surface coverage during the NH_3 half-reaction results in the growth of NH_2^* surface coverage that becomes equivalent to the NH_2^* surface coverage measured prior to the WF_6 half-reaction. These results indicate that the NH_3 and WF_6 surface reactions proceed to completion at 600 K with sufficient reactant exposure. In addition, each reaction is self-limiting and terminates with the consumption of the initial surface functional groups.

Infrared difference spectra were also recorded during the WF_6 and NH_3 half-reactions at 700 and 500 K. At 700 K, the WF_6 and NH_3 half-reactions were observed to be faster than at 600 K. However, conductance limitations in the high surface area silica powder prevented a quantitative description of the relative reaction rates. The half-reactions at 700 K were self-limiting and terminated with the consumption of the initial surface species. The integrated absorbances for the WF_6 and NH_3 half-reactions at 700 K showed that the initial loss of WF_x^* surface species during the NH_3 half-reaction did not correspond with a concurrent growth of NH_2^* surface species. This behavior is consistent with each NH_3 molecule initially reacting with even more WF_x^* surface species at 700 than at 600 K. In contrast, the WF_6 half-reaction at 700 K occurred with a concurrent gain of WF_x^* surface species and loss of NH_2^* surface species.

At 500 K, the NH_3 half-reaction was observed to saturate after removing only $\sim 60\%$ of the WF_x^* surface species. Larger NH_3 reactant exposures did not remove additional WF_x^* surface species. This behavior indicates that the NH_3 half-reaction does not proceed to completion at 500 K. In contrast, the WF_6 half-reaction was observed to consume all of the surface NH_2^* species resulting from the NH_3 reaction at 500 K. The WF_6 half-reaction at 500 K was also performed on a tungsten nitride surface that had earlier received a saturation exposure of NH_3 at 600 K. This experiment revealed that sufficient WF_6 exposures can consume all the NH_2^* surface species at 500 K. The inability of the NH_3 half-reaction to react with all WF_x^* surface species at 500 K indicates that tungsten nitride film growth should be performed at temperatures ≥ 600 K to obtain the best tungsten nitride films.

Spectroscopic ellipsometry studies of film growth.—The dependence of the half-reactions on the WF_6 and NH_3 reactant exposures was examined by measuring the tungsten nitride film thickness deposited by 3 AB cycles at 600 K. A typical AB cycle occurred with the following sequence: expose WF_6 (1-10 mTorr)/ N_2 purge 1-3 min/expose NH_3 (1-10 mTorr)/ N_2 purge 1-3 min. The ellipsometric measurements shown in Fig. 6 and 7 demonstrate that the WF_6 and NH_3 half-reactions are self-limiting at 600 K. Once a half-reaction reaches completion, additional reactant exposure produces no additional film growth.

Figure 6 displays the tungsten nitride film thickness obtained vs. NH_3 reactant exposure with a WF_6 reactant exposure of 4300 L. This WF_6 exposure is sufficient for a complete WF_6 half-reaction. Figure 6 shows that the NH_3 half-reaction is incomplete and the tungsten nitride film thickness deposited by three AB cycles is dependent on NH_3 reactant exposure for NH_3 exposures $< 10,000$ L. In contrast, additional NH_3 exposure results in no further tungsten nitride deposition for NH_3 exposures $\geq 10,000$ L. The surface reactions are complete and self-limiting in this regime. The error bars represent the 90% confidence limits determined by the uncertainty in the ellipsometric data. The solid line is intended only to guide the eye.

The film thicknesses measured in Fig. 7 were obtained with a variable WF_6 exposure and a NH_3 reactant exposure of 12,000 L. This NH_3 exposure is sufficient for a complete NH_3 half-reaction. Figure 7 shows that the tungsten nitride film thickness deposited by 3 AB cycles is dependent on the WF_6 reactant exposure for WF_6 exposures < 3000 L. In contrast, additional WF_6 reactant exposure

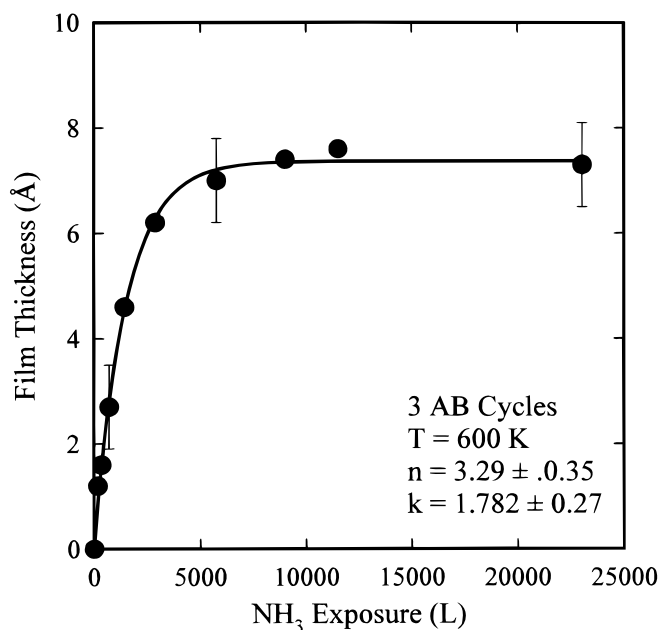


Figure 6. Ellipsometric measurements of the tungsten nitride film thickness deposited by three AB cycles vs. NH_3 exposure at 600 K. A WF_6 exposure of 4300 L was sufficient for a complete WF_6 half-reaction at 600 K.

results in no additional tungsten nitride deposition for WF_6 reactant exposures ≥ 3000 L.

Figure 8 shows the ellipsometric measurements of the tungsten nitride film thickness vs. the number of AB cycles at 600 K. The WF_6 reactant exposure of 4300 L and NH_3 reactant exposure of 12,000 L were sufficient for complete half-reactions during each AB cycle. The film thickness is directly proportional to the number of AB cycles. The solid line displays the least squares linear fit to the data.

The tungsten nitride film thickness vs. number of AB cycles is extremely linear. The least squares fit yields a growth rate of $2.55 \text{ \AA/AB cycle}$ at 600 K. This growth rate agrees well with the W_2N lattice constant of 2.4 \AA obtained by the X-ray diffraction (XRD) meas-

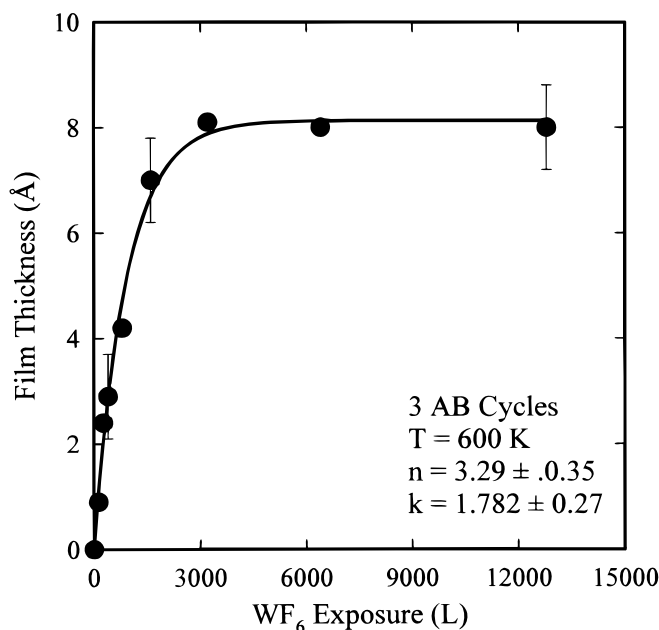


Figure 7. Ellipsometric measurements of the tungsten nitride film thickness deposited by three AB cycles vs. WF_6 exposure at 600 K. A NH_3 exposure of 12,000 L was sufficient for a complete NH_3 half-reaction at 600 K.

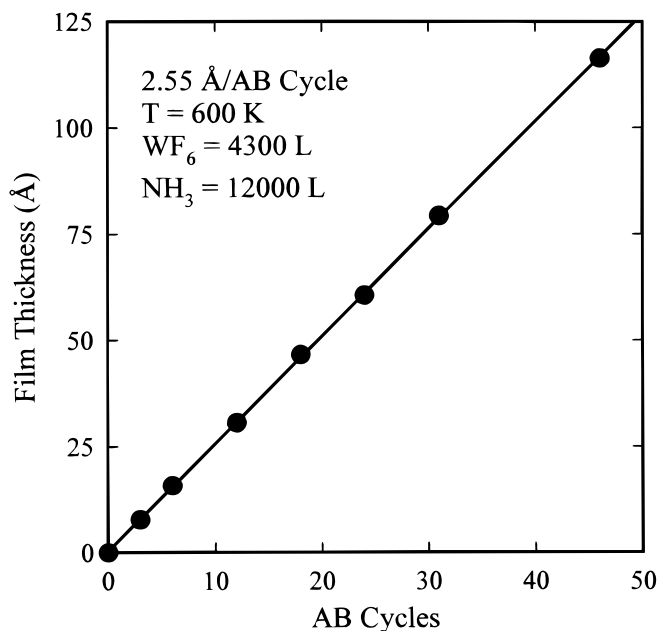


Figure 8. Tungsten nitride film thickness measured by ellipsometry vs. number of AB cycles at 600 K. The NH_3 exposure of 12,000 L and WF_6 exposure of 4300 L were sufficient for complete half-reactions during each AB cycle.

urements. The linear growth rate indicates that the number of reactive surface sites remains constant during tungsten nitride deposition. The constant growth rate also argues that the tungsten nitride films are growing with no surface roughening.

The ellipsometric measurements of the tungsten nitride film thickness deposited by three AB reaction cycles vs. substrate temperature are displayed in Fig. 9. The WF_6 and NH_3 reactant exposures at each temperature were sufficient for complete half-reactions and additional reactant exposure resulted in no further deposition. The solid line connects the data points, and the error bars represent the 90% confidence limits. Figure 9 shows that the tungsten nitride

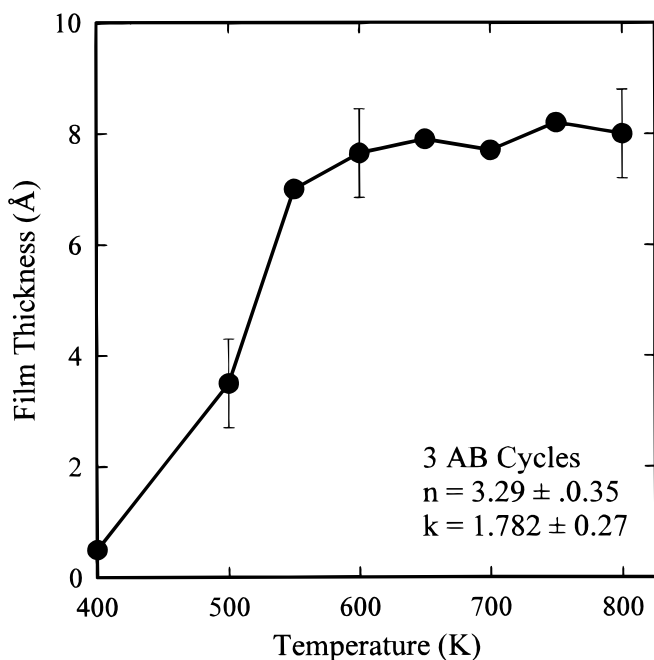


Figure 9. Ellipsometric measurements of the tungsten nitride film thickness deposited by three AB cycles at various substrate temperatures. Reactant exposures were sufficient for complete half-reactions at each temperature.

film thickness deposited by three AB cycles increases rapidly with substrate temperature from 400 to 600 K. In this temperature regime, the FTIR spectroscopy measurements indicate that the surface half-reactions do not proceed to completion and may produce a $\text{WF}_6\text{:NH}_3$ adduct species.

After the rapid rise vs. temperature from 400 to 600 K, the tungsten nitride film thickness deposited by 3 AB cycles increases only very slightly for substrate temperatures between 600-800 K. These temperatures are sufficient for complete half-reactions according to the FTIR vibrational studies. The nearly constant tungsten nitride deposition rate of ~ 2.5 Å/AB cycle for temperatures between 600 and 800 K is consistent with the thickness of a W_2N monolayer.

The surface topography of the deposited tungsten nitride films was examined with an atomic force microscope (AFM) operating in tapping mode (Digital Instruments-Nanoscope III). Figure 10 shows a 3.0 by 3.0 μm scan of a ~ 350 Å thick tungsten nitride film deposited by 140 AB cycles at 600 K. The reactant exposures were sufficient for both half-reactions to reach completion for all 140 AB cycles. The light-to-dark gray scale in Fig. 10 spans less than 25 Å.

The AFM images of the deposited tungsten nitride films exhibit a surface roughness of ± 6.1 Å (root-mean-square). In comparison, the surface roughness of the initial SiO_2 surface on Si(100) was ± 2.5 Å. The power spectral density of the surface roughness also exhibited the same statistical characteristics as the initial SiO_2 surface on Si(100).¹⁰ This smooth surface topography with a roughness comparable to the initial surface indicates that the tungsten nitride films are growing with negligible roughening.

The tungsten nitride film composition was evaluated using X-ray photoelectron spectroscopy (XPS) depth-profiling.^a The XPS depth-profiling experiments employed a 4 kV Ar^+ ion beam operating with a 10 mA/cm^2 ion current to sputter slowly through the 350 Å thick tungsten nitride film. The surface of the tungsten nitride film exhibited characteristic signals for W, C, N, F, and O atoms. After several minutes of sputtering through the surface region, the elemental concentrations in the bulk tungsten nitride film were constant until encountering the underlying SiO_2 film.

The XPS depth-profiling results revealed that the bulk tungsten nitride films had a W to N ratio of $\sim 3:1$. The films also contained small atomic percentage concentrations of $\sim 5\%$ C and $\sim 3.6\%$ O. These impurities may be attributed to CO dissociation resulting from the CO partial pressures in our diffusion-pumped central deposition

^a These experiments were performed by Eli Mateeva of the Department of Metallurgical and Materials Engineering at the Colorado School of Mines.

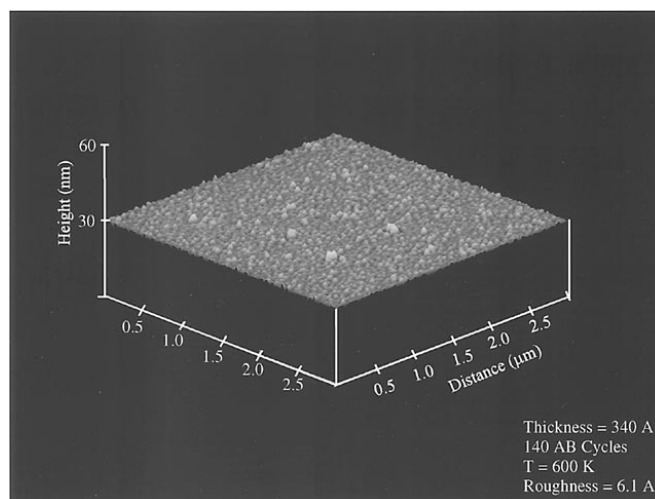


Figure 10. AFM image of a 350 Å thick tungsten nitride film deposited at 600 K after 140 AB cycles on a 125 Å thick SiO_2 film on Si(100). The reactant exposures of 12,000 L NH_3 and 4300 L WF_6 were sufficient for complete half-reactions during each AB cycle. The light-to-dark range is 25 Å.

chamber.³⁴ Alternatively, the impurities may result from artifacts encountered during Ar⁺ sputtering of metal and metal nitride films.³⁵ The large W:N ratio may result from the preferential removal of N atoms by Ar⁺ sputtering that is often observed for metal nitrides.³⁵

Glancing angle XRD experiments were also performed to evaluate the crystallographic structure of the tungsten nitride films. [See footnote ⁴ on the previous page.] Using Cu K α radiation incident at 4°, the tungsten nitride films displayed several diffraction peaks at angles 2 θ equal to 37, 43, and 63°. The most dominant peak was observed at 37°. These diffraction peaks are consistent with the (111), (200), (220) reflections of cubic W₂N.^{36,37} The estimated grain size of the W₂N crystallites determined from the width of the (111) diffraction peak was ~ 110 Å.

The adhesion of the tungsten films to the starting SiO₂ surface was qualitatively examined with the “adhesive tape test” procedure.³⁸ The tungsten nitride films survived the test with no evidence of delamination. The resistivity of the tungsten nitride films was also determined using a four-point probe apparatus with silver paint electrical contacts.³⁹ The measured resistivity was 4500 m Ω cm.

Discussion

Surface chemistry of tungsten nitride deposition.—The surface chemistry of tungsten nitride deposition can be studied by monitoring the vibrational absorption features of the NH₃^{*} and WF₆^{*} surface species. The N-H_y vibrational stretching region of the infrared spectra exhibits significant changes with reaction temperature. At 700 K, the N-H_y stretching region exhibited two sharp features at 3435 and 3515 cm⁻¹ that are assigned to the asymmetric and symmetric stretching modes of NH₂^{*} surface species. The N-H_y bending region displayed a strong peak at 1550 cm⁻¹ that is attributed to the N-H₂ scissors mode.^{29,30} The frequencies of these three modes are consistent with NH₂^{*} surface species with three-coordinate N atoms (W-NH₂).^{29,30} A small peak also appeared at 1485 cm⁻¹ that can be assigned to four-coordinate surface N atoms (W₂-NH₂).^{29,30}

Reduction of the reaction temperature to 600 K resulted in several new spectral features that are shown in Fig. 3 and 4. In addition to the 3435 and 3515 cm⁻¹ features observed at 700 K, the N-H₂ stretching region also displays two new features located at 3350 and 3290 cm⁻¹. In addition to the 1550 cm⁻¹ peak observed at 700 K, the N-H_y bending region also reveals a prominent 1485 cm⁻¹ feature and a weak 1610 cm⁻¹ feature. The additional infrared features at 600 K are attributed to NH₂^{*} surface species with four-coordinate N atoms (W₂-NH₂).^{29,30} These four-coordinate surface N atoms exist together with the three-coordinate surface N atoms. The 1610 cm⁻¹ feature is attributed to a small NH₃^{*} surface coverage.^{29,31}

Further changes in the N-H_y stretching and bending regions occur when the reaction temperature is lowered to 500 K. The three-coordinate N-H₂ stretching and bending modes are nearly extinguished at 3515, 3435, and 1550 cm⁻¹. In addition, the four-coordinate N-H₂ stretching and bending modes are persistent at 3350, 3290, and 1485 cm⁻¹. Two prominent spectral features are also observed at 3455 and 1610 cm⁻¹. These new features are attributed to molecular NH₃^{*} surface species.^{29,31} The presence of molecular NH₃^{*} surface species may indicate the formation of an WF₆:NH₃ adduct. This adduct has been observed earlier when using WF₆ and NH₃ reactants.²⁰ Tungsten nitride films that have incorporated the WF₆:NH₃ adduct exhibit poor adhesion and electrical properties.²⁰

The W-F_x stretching vibration in Fig. 3 and 4 is observed at ~ 680 cm⁻¹. This vibrational feature exhibited only subtle changes with reaction temperature. The W-F_x stretching mode broadened and shifted to slightly higher frequencies as the reaction temperature was lowered from 700 to 500 K. This frequency shift may be consistent with a higher coverage of surface fluorine species at lower reaction temperatures.

An analysis of the normalized integrated absorbance data presented in Fig. 5 yields additional details about the reactions at 600 K. In Fig. 5a, loss of WF₆^{*} surface coverage during the NH₃ half-reaction is coincident with the gain of NH₂^{*} surface coverage. Likewise, the loss of NH₂^{*} surface coverage in Fig. 5b is always concurrent

with the growth of WF₆^{*} surface coverage. This symmetry between loss and gain suggests that both the half-reactions occur in an approximately 1:1 fashion. The NH₃ reactant consumes WF₆^{*} surface species and deposits NH₂^{*} surface species. The WF₆ reactant consumes NH₂^{*} surface species and deposits WF₆^{*} surface species.

The FTIR spectra are consistent with self-limiting surface chemistry and the atomic layer controlled growth of tungsten nitride. The FTIR spectra do display some temperature dependence that may affect the deposited film stoichiometry. At 700 K during the NH₃ half-reaction, the WF₆^{*} surface coverage initially decreases with very little corresponding increase in the NH₂^{*} surface coverage. This observation suggests that each NH₃ molecule can react initially with multiple WF₆^{*} surface species at 700 K. During the WF₆ half-reaction at 700 K, the loss of NH₂^{*} surface coverage and gain of WF₆^{*} surface coverage are symmetrical and similar to the behavior observed at 600 K.

When the reaction temperature is lowered to 500 K, the NH₃ precursor cannot react with all of the WF₆^{*} surface species. This NH₃ half-reaction saturates after removing only ~ 60 % of the initial WF₆^{*} surface coverage. In contrast, the WF₆ half-reaction displays very symmetrical behavior at 500 K. The loss of N-H_y absorbance features and gain of W-F_x absorbance features are in close correspondence.

The temperature dependence of the NH₃ half-reaction suggests that the N content of the deposited tungsten nitride films may change with reaction temperature. A lower N content may be observed at 700 K because each NH₃ molecule can initially react with multiple WF₆^{*} surface species. This prediction is consistent with other studies that observe lower N concentrations in tungsten nitride films deposited at higher reaction temperatures.^{19,36,37} Likewise, a lower N content may also be measured at 500 K because the NH₃ half-reaction does not proceed to completion. These predictions should be tested by evaluating the stoichiometry of tungsten nitride films deposited at different substrate temperatures.

Tungsten nitride film growth on Si(100).—Figures 6 and 7 demonstrate the self-limiting nature of the NH₃ and WF₆ half-reactions at 600 K. These results reveal that NH₃ exposures of 10,000 L and WF₆ exposures of 3000 L are needed for complete surface half-reactions at 600 K. Using saturation exposures of NH₃ and WF₆, the deposited tungsten nitride thickness vs. number of AB reaction cycles was examined in Fig. 8. The film growth was extremely linear with a tungsten nitride deposition rate of 2.55 Å/AB cycle.

The linear growth observed in Fig. 8 indicates that the tungsten nitride films are growing very smoothly on the Si(100) substrate. The AFM image in Fig. 10 confirms the deposition of very smooth and uniform tungsten nitride films. The surface roughness of this tungsten nitride film is only ± 6.1 Å (root-mean-square). The slight roughness of this film may be attributed in part to the presence of small tungsten nitride crystallites.

Figure 9 reveals that the tungsten nitride deposition is very constant for temperatures ≥ 600 K. This constant deposition rate vs. temperature was not observed in earlier studies of Al₂O₃ and SiO₂ atomic layer controlled growth.^{10,11} This earlier temperature dependence was attributed to the loss of hydroxyl groups on Al₂O₃ and SiO₂ by dehydroxylation.^{40,41} The constant tungsten nitride deposition rate vs. temperature may result from the higher thermal stability of the WF₆^{*} and NH₂^{*} surface species. If the WF₆^{*} and NH₂^{*} surface coverages remain constant at ≥ 600 K, the same number of tungsten and nitrogen atoms should be deposited each AB cycle.

The spectroscopic ellipsometric measurements determined that the real and imaginary refractive index ($\tilde{n} = n + ik$) varied with film thickness. The refractive index was $n = 2.2 \pm 0.6$ and $k = 0.7 \pm 0.3$ at $\lambda = 632$ nm for a 45 Å thick tungsten nitride film. The refractive index was $n = 3.29 \pm 0.35$ and $k = 1.78 \pm 0.27$ at $\lambda = 632$ nm for a 275 Å thick film. Tungsten nitride film thicknesses ≥ 275 Å resulted in no further change in the refractive index.

The changing refractive index with film thickness may simply result from the evolution of the electronic band structure with film thickness. The film composition is not believed to vary vs. film

thickness because the tungsten nitride deposition rate per AB cycle remained constant vs. film thickness. The measured optical constants for the thick tungsten nitride films ≥ 275 Å are consistent with tungsten nitride films that have a W:N ratio between 2:1 and 1:1.⁴² Tungsten nitride films thicker than ~ 500 Å could not be measured using ellipsometry because of strong light absorption by the metallic film.

Tungsten nitride films commonly exist as W_2N or WN with a 2:1 or 1:1 W/N stoichiometry.³⁶ A 1:2 W/N stoichiometry is unlikely because the WN_2 structure is very unstable. The tungsten nitride crystal structure consists of a face centered cubic (fcc) sublattice of W atoms. Half of the octahedral holes are filled with N atoms in the W_2N structure. All of the octahedral holes are filled with N atoms in the WN structure. These arrangements produce a cubic crystal lattice for W_2N and a hexagonal lattice structure for WN.⁴³ The cubic crystal lattice for W_2N is the most stable structure and is almost always observed in tungsten nitride film growth studies.^{6,20,23} The heat of formation of -5.3 kcal/mol for W_2N is slightly more exothermic than the heat of formation of -3.6 kcal/mol for WN.⁵

The XRD measurements of the tungsten nitride films revealed mainly cubic W_2N with a dominant (111) peak. The lattice constant derived from the (111) peak was ~ 2.4 Å. This lattice constant agrees with the tungsten nitride growth rate of 2.55 Å/AB cycle obtained from the measurements shown in Fig. 8. The grain size of the tungsten nitride films was estimated to be ~ 110 Å from the (111) diffraction peak. These X-ray results indicate that the tungsten nitride films have not developed a large grain crystallized structure. The AFM measurements shown in Fig. 10 may be observing some small crystallites on the tungsten nitride surface that are consistent with the XRD results. Small crystalline grains are commonly observed in tungsten nitride films grown at low temperature.^{2,6}

The 3:1 W/N stoichiometry determined by the XPS sputter depth-profiling measurements is in disagreement with the XRD analysis that indicated a W_2N film stoichiometry. Similar disagreement has been observed in other tungsten nitride film growth studies.^{19,37} These studies have also observed W_2N by XRD and measured either higher or lower W/N stoichiometry by Ar^+ sputter profiling.^{19,37} Ar^+ ion beam sputtering usually results in preferential removal of N atoms that yields artificially high W:N ratios.³⁵ Extra N atoms are also believed to exist at grain boundaries between tungsten nitride crystallites.^{2,37} These extra N atoms at the grain boundaries are not observed by the XRD experiment and may contribute to a lower W:N ratio measured during sputter depth-profiling.

Conclusions

The atomic layer deposition of tungsten nitride films was demonstrated using self-limiting sequential surface reactions. Alternating exposures of NH_3 and WF_6 in an ABAB... reaction sequence were used to deposit the tungsten nitride films. Transmission FTIR spectroscopy studies indicated that the NH_3 and WF_6 surface reactions were complete and self-limiting at $T \geq 600$ K. *In situ* spectroscopic ellipsometry measurements determined that the tungsten nitride growth per AB cycle was extremely linear with growth rates of ~ 2.5 Å/AB cycle at 600-800 K.

AFM images revealed that the deposited tungsten nitride films were exceptionally flat with a roughness similar to the initial surface. XRD experiments revealed the films consisted of small W_2N crystallites with a diameter ~ 110 Å and a preferred (111) orientation. XPS depth-profiling measurements of the tungsten nitride films observed only low C, O, and F impurity concentrations. The atomic layer deposition of smooth tungsten nitride films should find many applications and may be particularly important as a diffusion barrier for Cu on contact and via holes.

Acknowledgments

This work was supported in part by Advanced Micro Devices through a graduate student fellowship for J.W.K. Additional support was received from the Air Force Office of Scientific Research. Some of the equipment utilized in this investigation was provided by earlier support from the Office of Naval Research. The authors thank Dr. Tom Seidel of Genus, Inc., in Sunnyvale, CA, for motivating this research and contributing many helpful suggestions.

The University of Colorado at Boulder assisted in meeting the publication costs of this article.

References

1. *The National Technology Roadmap for Semiconductors*, SIA Semiconductor Industry Association, San Jose, CA (1997).
2. M. Takeyama and A. Noya, *Jpn. J. Appl. Phys.*, **36**, 2261 (1997).
3. U. Masaki, O. Takeo, M. Masanori, T. Katsumi, Y. Sadae, N. Tadashi, and O. Tomohiro, *Thin Solid Films*, **286**, 170 (1996).
4. T. Mayumi and N. Atsushi, *Jpn. J. Appl. Phys.*, **36**, 2261 (1997).
5. M. Uekubo, T. Oku, K. Nii, M. Murakami, K. Takahiro, S. Yamaguchi, T. Nakano, and T. Ohta, *Thin Solid Films*, **286**, 170 (1996).
6. B. Park, D. Ko, Y. Kim, J. Ha, Y. Park, S. Lee, H. Lee, M. Lee, U. Chung, Y. Koh, and M. Lee, *J. Appl. Mater.*, **26**, L1 (1997).
7. S. M. George, A. W. Ott, and J. W. Klaus, *J. Phys. Chem.*, **100**, 13121 (1996).
8. C. H. L. Goodman and M. V. Pessa, *J. Appl. Phys.*, **60**, R65 (1986).
9. T. Suntola, *Thin Solid Films*, **216**, 84 (1992).
10. A. W. Ott, J. W. Klaus, J. M. Johnson, and S. M. George, *Thin Solid Films*, **292**, 135 (1996).
11. J. W. Klaus, A. W. Ott, J. M. Johnson, and S. M. George, *Appl. Phys. Lett.*, **70**, 1092 (1997).
12. J. W. Klaus, O. Sneh, and S. M. George, *Science*, **278**, 1934 (1997).
13. H. Kumagai, K. Toyoda, K. Kobayashi, M. Obara, and Y. Iimura, *Appl. Phys. Lett.*, **70**, 2338 (1997).
14. K. Kukli, J. Ihanus, M. Ritala, and M. Leskela, *Appl. Phys. Lett.*, **68**, 3737 (1996).
15. J. W. Klaus, A. W. Ott, A. Dillon, and S. M. George, *Surf. Sci. Lett.*, **418**, L14 (1998).
16. M. Han, Y. Luo, J. E. Moryl, J. G. Chen, and R. M. Osgood, *Surf. Sci.*, **415**, 251 (1998).
17. M. Ishii, S. Iwai, H. Kawata, T. Ueki, and Y. Aoyagi, *J. Cryst. Growth*, **180**, 15 (1997).
18. J. W. Klaus, S. J. Ferro, and S. M. George, *Thin Solid Films*, In press (2000).
19. S. Marcus and R. Foster, *Thin Solid Films*, **236**, 330 (1993).
20. T. Nakajima, K. Watanabe, and N. Watanabe, *J. Electrochem. Soc.*, **134**, 3175 (1987).
21. C. Meunier, C. Monteil, C. Savall, F. Palmino, J. Weber, R. Berjoan, and J. Durand, *Appl. Surf. Sci.*, **125**, 313 (1998).
22. C. W. Lee, Y. T. Kim, and S. K. Min, *Appl. Phys. Lett.*, **62**, 3312 (1993).
23. Y. T. Kim and S. K. Min, *Appl. Phys. Lett.*, **59**, 929 (1991).
24. A. C. Dillon, M. B. Robinson, M. Y. Han, and S. M. George, *J. Electrochem. Soc.*, **139**, 537 (1992).
25. P. Basu, T. H. Ballinger, and J. T. Yates Jr., *Rev. Sci. Instrum.*, **59**, 1321 (1988).
26. O. Sneh, M. L. Wise, A. W. Ott, L. A. Okada, and S. M. George, *Surf. Sci.*, **334**, 135 (1995).
27. J. R. Creighton, *J. Vac. Sci. Technol. A*, **7**, 621 (1989).
28. N. Kobayashi, Y. Nakamura, H. Goto, and Y. Homma, *J. Appl. Phys.*, **73**, 4637 (1993).
29. M. Bartram, T. Michalske, J. Rogers, and T. Mayer, *Chem. Mater.*, **3**, 953 (1991).
30. D. Bertolet and J. Rogers, *Chem. Mater.*, **5**, 391 (1993).
31. K. Nakamoto, *Infrared Spectra of Inorganic and Coordination Compounds*, Wiley-Interscience, New York (1970).
32. G. E. Jellison, Jr., *Thin Solid Films*, **234**, 416 (1993).
33. *Guide to Using WVASE32*, J.A. Woollam Co., Inc., Lincoln, NE 6850 (1994).
34. E. Umbach and D. Menzel, *Surf. Sci.*, **135**, 199 (1983).
35. S. Ingrey, M. Johnson, R. Streater, and S. G., *J. Vac. Sci. Technol.*, **20**, 968 (1982).
36. H. T. Chiu and S. H. Chuang, *J. Mater. Res.*, **8**, 1353 (1993).
37. M. Tsai, S. Sun, H. Chiu, and S. Chuang, *Appl. Phys. Lett.*, **68**, 1412 (1996).
38. B. N. Chapman, *J. Vac. Sci. Technol.*, **11**, 106 (1974).
39. I. B. Valdes, *Proc. Inst. Radio Engrs.*, **42**, 420 (1954).
40. A. W. Ott, K. C. McCarley, J. W. Klaus, J. D. Way, and S. M. George, *Appl. Surf. Sci.*, **107**, 128 (1996).
41. O. Sneh and S. M. George, *J. Phys. Chem.*, **99**, 4639 (1994).
42. P. Boher, P. Houdy, P. Kaikati, and L. J. Van Ijzendoorn, *J. Vac. Sci. Technol. A*, **8**, 846 (1989).
43. *International Tables for X-Ray Crystallography*, D. Reidel, Dordrecht (1983).